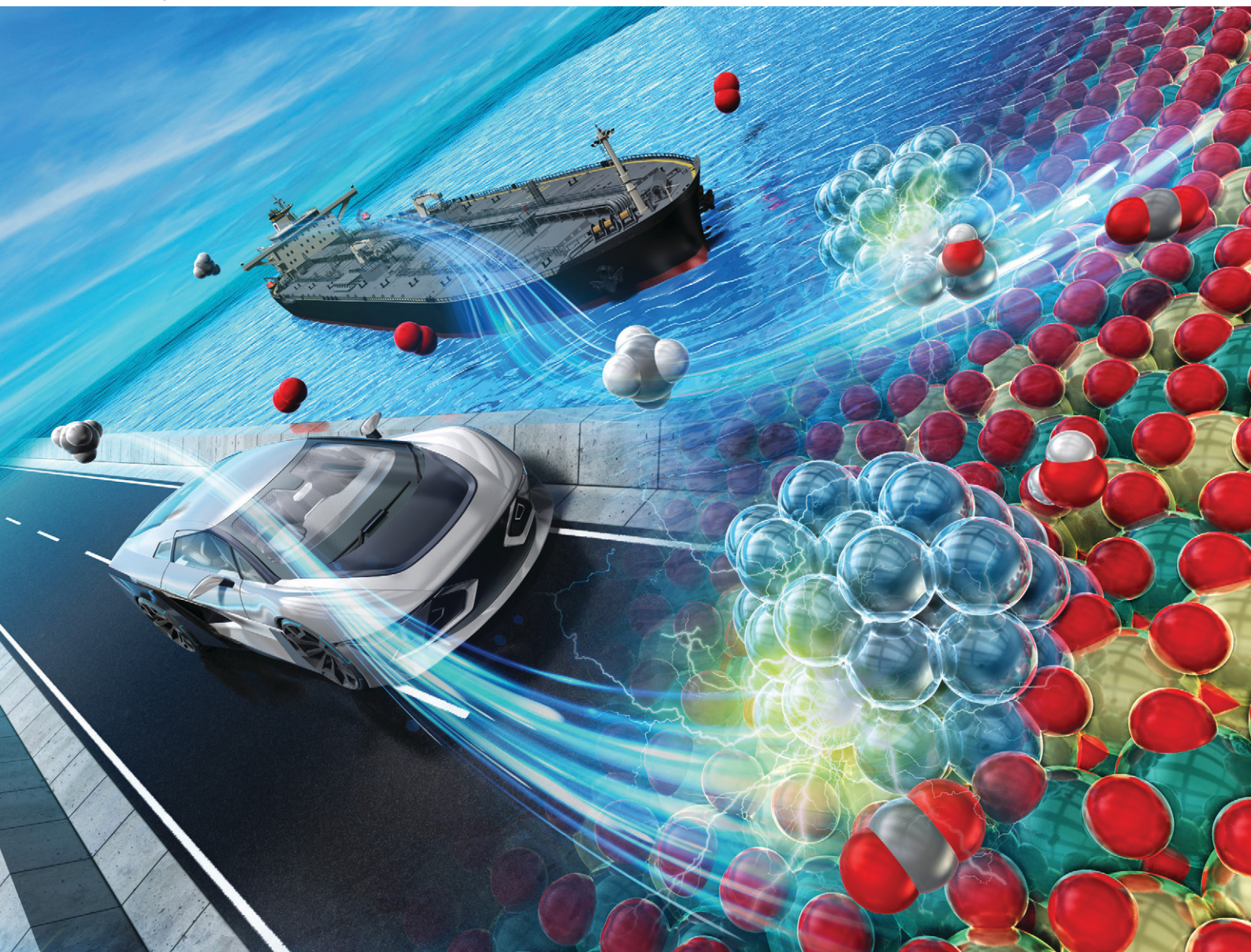


# Catalysis Science & Technology

Volume 14  
Number 23  
7 December 2024  
Pages 6723–6970

rsc.li/catalysis



ISSN 2044-4761

**PAPER**

Yasushi Sekine *et al.*

Synergistic effect of Pd/CZO catalysts and an electric field on complete combustion of lean and humid methane at low temperatures

Cite this: *Catal. Sci. Technol.*, 2024,  
14, 6775

# Synergistic effect of Pd/CZO catalysts and an electric field on complete combustion of lean and humid methane at low temperatures†

Kei Sugiura,<sup>ab</sup> Takuma Higo,<sup>id</sup> Nobuki Matsumoto,<sup>a</sup>  
Harunobu Tedzuka<sup>a</sup> and Yasushi Sekine<sup>id</sup>\*<sup>a</sup>

The elimination of unburned methane produced by internal combustion engines is extremely important because of the strong greenhouse effect of methane. Difficulties in controlling unburned methane arise from its characteristics, such as its difficulty of adsorption, low exhaust gas temperatures in an efficient engine, low concentrations of unburned emitted methane, and the coexistence of steam and residual oxygen as coexisting substances in the exit gas. Results of the present study demonstrate that the removal activity of methane by complete combustion was improved dramatically at low temperatures by the application of a DC electric field to the Pd/Ce<sub>x</sub>Zr<sub>1-x</sub>O<sub>2</sub> catalyst system, even under a humid atmosphere. Specifically, 1 wt% Pd/Ce<sub>0.25</sub>Zr<sub>0.75</sub>O<sub>2</sub> showed very higher methane conversion under humid conditions than under dry conditions at 473 K in the presence of an electric field. To elucidate the reaction mechanisms involved in this process of steam adsorption, we conducted partial pressure dependence tests and activity tests with steam under an electric field.

Received 2nd June 2024,  
Accepted 25th August 2024

DOI: 10.1039/d4cy00699b

rsc.li/catalysis

## Introduction

Methane is widely used as a fuel for vehicles and maritime vessels because of its cost-effectiveness and lower carbon dioxide emissions than either diesel oil or heavy oil.<sup>1–4</sup> Nevertheless, methane, itself a greenhouse gas, is about 28 times more influential as a greenhouse gas than carbon dioxide.<sup>5,6</sup> Effective control of residual, non-combusted methane emitted from natural gas engines is therefore an extremely important issue for global warming prevention. Consequently, the catalytic complete oxidation of methane has attracted much attention over the past two decades.<sup>7–10</sup> This reaction is represented by the following equation.



Because methane is stable and activating its C–H bond is difficult, low exhaust gas temperatures (below 573 K) pose challenges for the complete combustion and removal of methane through exhaust gas purification of natural gas engines.<sup>11,12</sup>

Earlier reports have described that Pd-based catalysts,<sup>13,14</sup> which show high performance for methane combustion, can only slightly reduce the light-off temperature  $T_{50}$  (the temperature required for methane conversion to reach 50%) below 573 K. Furthermore, it has been revealed that the activity of Pd-based catalysts decreases in the presence of steam, which coexists in exhaust emissions from natural gas engines, comprising approximately 10–15%.<sup>15</sup>

To overcome this difficulty, non-conventional catalytic processes have been investigated: non-equilibrium plasma systems, non-faradic electrochemical modification of catalytic activity (NEMCA) systems, and other electrochemical processes represent methods for providing additional energy input to enhance catalytic methane activation.<sup>16,17</sup> Nevertheless, these systems typically exhibit high energy consumption. To mitigate this consumption difficulty, catalytic processes in an electric field have been proposed.<sup>18–23</sup> Using such processes, catalytic steam reforming and catalytic NO<sub>x</sub> reduction can proceed even at low temperatures with low energy consumption.<sup>20,22,23</sup> These results suggest that the electric field can promote the activation of methane and water, even at 423 K. Li *et al.* used this approach for the methane complete combustion in a dry condition over a Pd/CZO catalyst, achieving high methane conversion at 573 K.<sup>24</sup>

For this study, we have investigated the complete oxidation of methane using Pd/CZO catalysts with the electric field under humid conditions. Results demonstrated that 1 wt% Pd/Ce<sub>0.25</sub>Zr<sub>0.75</sub>O<sub>2</sub> catalyst exhibited superior activity

<sup>a</sup> Applied Chemistry, Waseda University, 3-4-1, Okubo, Shinjuku, Tokyo, Japan.

E-mail: ysekine@waseda.jp

<sup>b</sup> RD Center, N.E. CHEMCAT Corporation, 678, Ipponmatsu, Numazu, Shizuoka, Japan. E-mail: kei.sugiura@ne-chemcat.co.jp† Electronic supplementary information (ESI) available. See DOI: <https://doi.org/10.1039/d4cy00699b>

compared to the earlier reported catalysts in a 1 mA electric field at 473 K with 10% H<sub>2</sub>O. The methane conversion was better than that achieved under dry conditions. Moreover, H<sub>2</sub>O-TPD analysis revealed that 1 wt% Pd/Ce<sub>0.25</sub>Zr<sub>0.75</sub>O<sub>2</sub> showed high water resistance. Partial pressure dependence tests and methane activation tests with steam provided insight into the relation between methane and steam on the catalytic surface.

## Experimental

### Catalyst preparation

Ce<sub>x</sub>Zr<sub>1-x</sub>O<sub>2</sub> ( $x = 0, 0.25, 0.5, 0.75, 0.9$ ) was synthesised using a polymerised complex method with citric acid and ethylene glycol.<sup>23</sup> After citric acid, ethylene glycol, Ce(NO<sub>3</sub>)<sub>3</sub>·6H<sub>2</sub>O and ZrO(NO<sub>3</sub>)<sub>2</sub>·6H<sub>2</sub>O (Kanto Chemical Co. Inc.) were dissolved into 250 mL water, the solution was stirred in a water bath at 353 K overnight. Then the mixture was dried up on a hot plate with stirring. The molar ratio of metal: citric acid: ethylene glycol was 1:3:3. The dried-up powder was calcined at 673 K for 4 h as pre-calcination and finally calcined at 973 K for 5 h.

Then 1 wt% Pd/Ce<sub>x</sub>Zr<sub>1-x</sub>O<sub>2</sub> was prepared *via* an impregnation method. After Ce<sub>x</sub>Zr<sub>1-x</sub>O<sub>2</sub> and 30 mL acetone were added to a 300 mL flask, the mixture was stirred for 2 h using a rotary evaporator. Palladium acetate (Kanto Chemical Co. Inc.) was dissolved into an acetone solution. Finally, the resulting solution was stirred for 2 h. After the suspension was dried up on a hot plate with stirring, the resultant powder was calcined at 393 K overnight as pre-calcination. The pre-calcined powder was calcined at 773 K for 3 h. The powders were sieved to obtain particles of 355–500 μm for activity tests.

Due to the low electron conductivity and resulting discharge in the case of 1 wt% Pd/ZrO<sub>2</sub> ( $x = 0$ ), the results of 1 wt% Pd/Ce<sub>x</sub>Zr<sub>1-x</sub>O<sub>2</sub> ( $x = 0.25, 0.5, 0.75, 0.9$ ) were presented in this paper.

### Activity tests

Catalyst performance tests with the electric field were conducted using a fixed bed flow-type reactor equipped with a DC power supply, as illustrated in Fig. S1 (ESI†).<sup>21</sup> Two stainless steel rods (2.0 mm i.d.) were inserted into a quartz tube (6.0 mm i.d.) to serve as electrodes. The imposed DC current was 1 mA. The voltage was dependent on the conductivity of the catalysts. The electric profiles were recorded using an oscilloscope (TBS 2000B Series; Tektronix Inc.). The furnace temperature was maintained as higher than 373 K to prevent water condensation and the experiments were conducted so that the furnace temperature remained constant for each test temperature. Approximately 120 mg of catalyst samples were used for each performance test without any pretreatment. The ratio of reactant feed gases in the complete methane combustion was CH<sub>4</sub>:O<sub>2</sub>:H<sub>2</sub>O:N<sub>2</sub> = 0.2:10:y:89.8 - y ( $y = 0, 1, 2.5$  and 10). The total flow rate was controlled at 50 mL min<sup>-1</sup> and gas hourly space

velocity (GHSV) was 20 000 h<sup>-1</sup> unless otherwise specified. Product gases were analysed using GC-FID (GC-8A; Shimadzu Corp.) equipped with a GP-54 packed column and GC-TCD (GC-8A; Shimadzu Corp.) equipped with a molecular sieve 5A packed column. The formula for calculating methane conversion is shown below.

$$\text{Methane conversion [\%]} = \frac{F_{\text{Methane, in}} - F_{\text{Methane, out}}}{F_{\text{Methane, in}}} \times 100 \quad (2)$$

Therein,  $F_{\text{Methane, in}}$  and  $F_{\text{Methane, out}}$  respectively represent the CH<sub>4</sub> flow rate of the inlet and outlet. In tests for methane activation with steam, a gas composition of CH<sub>4</sub>:H<sub>2</sub>O:N<sub>2</sub> = 0.2:10:89.8 was used. Other conditions were set as the same to those of the complete methane combustion tests. The carbon balance in the activity tests ranged from 90% to 110%.

### Characterisation

The crystalline structures of prepared catalysts were characterised using powder X-ray diffraction (Smart Lab; Rigaku Corp.) operating at 40 kV and 40 mA with Cu K<sub>α</sub> radiation. The  $2\theta$  angle was set as 20–90 degrees. The lattice spacing calculated using Bragg's law from CZ (111) phase and the lattice constant assuming a cubic crystal structure are shown in Table S1 (ESI†).

The specific surface area of each catalyst was determined by N<sub>2</sub> adsorption using the Brunauer–Emmett–Teller (BET) method with a specific surface area analyser (Gemini VII; Micromeritics Instrument Corp.).

Using a catalyst analyser (BELCAT II; Microtrac BEL Corp.), CO-pulse measurements for ascertaining the particle size of the supported Pd were conducted. Before measurement, pretreatment of catalysts at 673 K was conducted for 15 min in a helium atmosphere. Then CO pulses were introduced at 323 K until the detected CO signal was stabilised. The Pd particle size was calculated from the amount of CO adsorption assuming adsorption stoichiometry of CO/Pd = 1.

The water adsorption amount was evaluated with a catalyst analyser (BELCAT-A; Microtrac BEL Corp.) employing temperature-programmed desorption analysis (H<sub>2</sub>O-TPD). The samples were calcined at 773 K in 1% O<sub>2</sub>/helium atmosphere. Water was introduced for 1 h at 353 K. After the physically adsorbed water was removed under helium flow, TPD was conducted under a helium atmosphere at a heating rate of 20 K min<sup>-1</sup>, with gas detection using a TCD.

The Pd particle structure was examined using field emission scanning transmission electron microscopy (JEM-ARM200F; JEOL) at 200 kV. Energy dispersive X-ray spectroscopy (EDS) mapping was used to observe the state of Pd particle distribution.

The electronic state of Pd of catalysts was measured using X-ray photoelectron spectroscopy (XPS, Quantera SXM; ULVAC-PHI Inc.) with a monochromatic Al-K<sub>α</sub> X-ray source. For the as-made samples, no pretreatment was applied. For the spent catalysts, the catalysts were operated under the



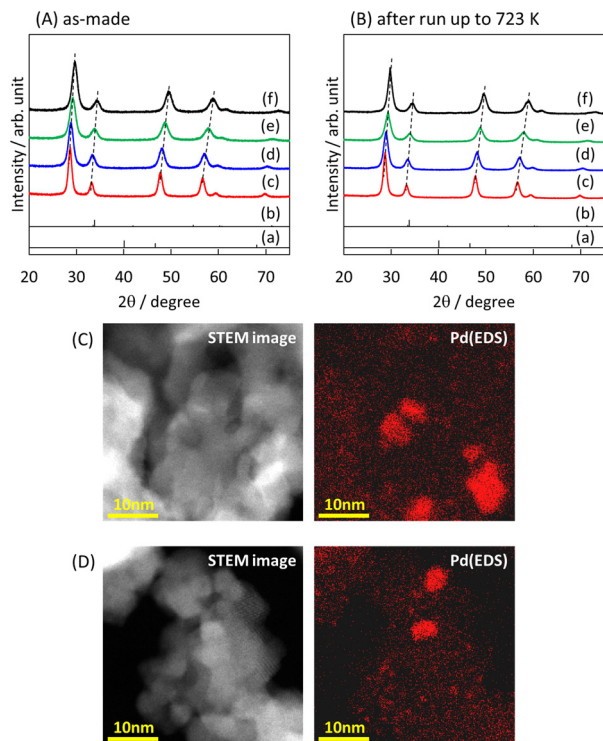


**Fig. 1** XRD pattern of 1 wt% Pd/Ce<sub>x</sub>Zr<sub>1-x</sub>O<sub>2</sub>: (A) as-made and (B) after run operated in the humid conditions with the electric field (1 mA) up to 723 K, with (a) Pd #46-1043, (b) PdO #41-1107, (c)  $x = 0.9$ , (d)  $x = 0.75$ , (e)  $x = 0.5$ , and (f)  $x = 0.25$ ; STEM images/EDS mappings for (C) 1 wt% Pd/Ce<sub>0.25</sub>Zr<sub>0.75</sub>O<sub>2</sub> and (D) 1 wt% Pd/Ce<sub>0.75</sub>Zr<sub>0.25</sub>O<sub>2</sub> as-made.

humid conditions with the electric field (1 mA) up to 723 K. The obtained binding energies were calibrated by C 1s at 284.6 eV. The distributions of Pd (~335.9 eV) and PdO (~337.1 eV) were calculated from the respective peak areas of 3d<sub>5/2</sub>. The results are presented in Fig. S2 (ESI†).

The effects of water in complete methane combustion were estimated using H<sub>2</sub><sup>18</sup>O. Methane, oxygen, H<sub>2</sub><sup>16</sup>O mixed with H<sub>2</sub><sup>18</sup>O (H<sub>2</sub><sup>16</sup>O:H<sub>2</sub><sup>18</sup>O = 3:2), Ar, and balanced N<sub>2</sub> were fed to the reactor at 50 mL min<sup>-1</sup> (CH<sub>4</sub>:O<sub>2</sub>:H<sub>2</sub>O:Ar:N<sub>2</sub> = 0.2:10:10:19.8:60). Also, C<sup>16</sup>O<sub>2</sub> ( $m/z = 44$ ), C<sup>16</sup>O<sup>18</sup>O ( $m/z = 46$ ), C<sup>18</sup>O<sub>2</sub> ( $m/z = 48$ ), and Ar ( $m/z = 40$ ) were detected using a quadrupole mass spectrometer. As shown in Table S2,† the selectivity to CO was low in activity tests, with the selectivity to CO<sub>2</sub> exceeding 99%. Therefore, CO and N<sub>2</sub> ( $m/z = 28$ ) was not evaluated in this isotopic test.

## Results and discussion

### Characterisation of prepared catalysts

Fig. 1(A) and (B) present XRD patterns of the as-made and after reaction of 1 wt% Pd/Ce<sub>x</sub>Zr<sub>1-x</sub>O<sub>2</sub> ( $x = 0.25, 0.5, 0.75, 0.9$ ) catalysts. These XRD diffraction patterns exhibited peaks attributed to CeO<sub>2</sub>-ZrO<sub>2</sub>. The observed peak shift toward higher angles with increasing Zr content suggests the formation of a solid solution of CeO<sub>2</sub>-ZrO<sub>2</sub>. No peak corresponding to Pd and PdO was observed in any XRD pattern. These findings indicate that the supported palladium is highly dispersed in all samples.

Table 1 presents the BET specific surface areas by N<sub>2</sub> adsorption, along with the amount of CO adsorption and the Pd particle sizes determined through CO-pulse measurements. The specific surface area decreased concomitantly with increasing amounts of Zr addition. By contrast, the amount of CO adsorption was at the same level for all samples, showing no dependence on the specific surface area or the oxide structure. Additionally, assuming adsorption stoichiometry of CO/Pd = 1, the Pd particle size was approximately 2 nm for all samples. Table 1 also provides the adsorption amounts of water per surface area measured using H<sub>2</sub>O-TPD. The water desorption profiles are presented in Fig. S3 (ESI†). The effects of water adsorption on the activity are discussed later herein.

Fig. 1(C) and (D) show the observation of Pd particles on CeO<sub>2</sub>-ZrO<sub>2</sub> using FE-STEM. In the STEM images, the presence of Pd nanoparticles was confirmed. Therefore, the findings suggest that Pd exists in a highly dispersed on CeO<sub>2</sub>-ZrO<sub>2</sub>, irrespective of the Ce/Zr ratio.

### Evaluation of methane complete combustion in humid conditions

The complete combustion of methane over 1 wt% Pd/Ce<sub>0.25</sub>-Zr<sub>0.75</sub>O<sub>2</sub> was evaluated with and without the electric field at various temperatures. The current was set to 1 mA based on the current variation test (Fig. S4, ESI†) that while the methane conversion improved with increased current, the energy efficiency decreased due to losses from Joule heating. Fig. 2(a) presents methane conversion at 473–773 K. As expected, the catalytic reaction with the electric field assists the methane oxidation from low temperatures. Results demonstrate that  $T_{50}$  without the electric field was about 650 K: with the electric field, it was less than 473 K. Consequently, it was confirmed that the application of the electric field reduces  $T_{50}$  by approximately

**Table 1** BET specific surface area, amount of CO adsorption, Pd particle size, and water adsorption amount per surface area in as-made

Samples	BET surface area/m <sup>2</sup> g <sup>-1</sup>	Amount of CO adsorption/cm <sup>3</sup> g-cat <sup>-1</sup>	Average Pd particle size/nm	Water adsorption amount per surface area/μmol m <sup>-2</sup>		
				First peak (343–473 K)	Second peak (473–773 K)	Total
1 wt% Pd/Ce <sub>0.25</sub> Zr <sub>0.75</sub> O <sub>2</sub>	28.0	1.57	1.5	0.406	0.464	0.870
1 wt% Pd/Ce <sub>0.5</sub> Zr <sub>0.5</sub> O <sub>2</sub>	20.8	1.14	2.1	0.487	0.592	1.079
1 wt% Pd/Ce <sub>0.75</sub> Zr <sub>0.25</sub> O <sub>2</sub>	22.6	1.30	1.8	0.508	0.772	1.280
1 wt% Pd/Ce <sub>0.9</sub> Zr <sub>0.1</sub> O <sub>2</sub>	48.1	1.51	1.6	0.411	0.480	0.891



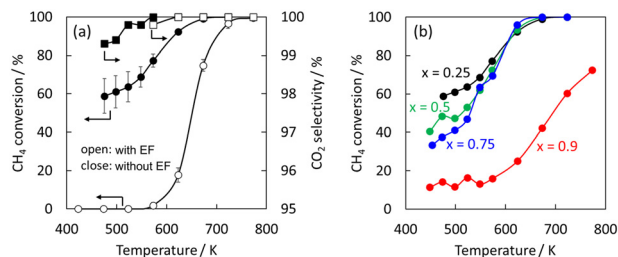


**Fig. 2** (a) The results of activity tests over 1 wt% Pd/Ce<sub>0.25</sub>Zr<sub>0.75</sub>O<sub>2</sub>, ○: CH<sub>4</sub> conversion, □: CO<sub>2</sub> selectivity, CH<sub>4</sub>: 2000 ppm, O<sub>2</sub>: 10%, H<sub>2</sub>O: 10%, N<sub>2</sub> balance; (b) methane conversion over 1 wt% Pd/Ce<sub>x</sub>Zr<sub>1-x</sub>O<sub>2</sub> with the EF, CH<sub>4</sub>: 2000 ppm, O<sub>2</sub>: 10%, H<sub>2</sub>O: 10%, N<sub>2</sub> balance.

200 K or more. The voltage applied by the electric field is correlated with the conductivity of the catalysts at each temperature, as summarised in Table S2.† As has already been shown in many catalytic reactions in the electric field,<sup>18–23</sup> the effect of the temperature increase by the Joule heating due to the application of the electric field is negligible for the increase in temperature, and the activity increase at such a small power (1 mA, 1.5–1.9 kV, so less than 2 W in total). Therefore, such a significant increase in activity is brought by the electric field. Regarding energy consumption, the reaction with the electric field at 473 K required a total of 12.4 W (1.9 W by the electric field and 10.5 W by the external heating with a furnace). In contrast, the thermal reaction at 650 K, which exhibited comparable activity to the electric field catalysis, required 20.6 W by the external heating. Thus, the application of the electric field significantly reduced the energy consumption by approximately 8 W in our specific case.

The methane combustion activities on various supports of different Ce/Zr ratios were also investigated. The results are shown in Fig. 2(b). 1 wt% Pd/Ce<sub>0.9</sub>Zr<sub>0.1</sub>O<sub>2</sub> exhibited the least methane combustion activity, but it was observed that methane conversion improved with the increasing Zr ratio. Under humid conditions (H<sub>2</sub>O: 10%), 1 wt% Pd/Ce<sub>0.25</sub>Zr<sub>0.75</sub>O<sub>2</sub> demonstrated superior performance. As shown in Fig. S5 (ESI†), the catalyst showed no such high activity in the thermal reaction, but the methane combustion activity was enhanced considerably by the application of an electric field.

Fig. S6 in ESI† shows the methane combustion activity on the support only (Ce<sub>0.25</sub>Zr<sub>0.75</sub>O<sub>2</sub>) with and without the electric field. The activity was very low, with methane conversion of 7.9% for the thermal reaction and 14.5% for the reaction in the electric field. As with previous studies,<sup>13,14</sup> the presence of Pd was essential for high methane combustion activity in this system.

### Comparison of methane combustion activity under humid and dry conditions

As with humid conditions, the effect of the Ce/Zr ratio in the support was evaluated under dry conditions with and without the electric field (Fig. S7, ESI†). It was also confirmed that methane combustion activity significantly improved with the

electric field under dry conditions. Additionally, regardless of the presence of the electric field, 1 wt% Pd/Ce<sub>0.75</sub>Zr<sub>0.25</sub>O<sub>2</sub> exhibited the highest performance, and the activity order based on Ce/Zr ratio was consistent with the report of K. Li *et al.*<sup>24</sup> The effect of the electric field under dry conditions was also discussed in their paper. Focusing on 1 wt% Pd/Ce<sub>0.25</sub>Zr<sub>0.75</sub>O<sub>2</sub>, though this catalyst showed the third highest activity under dry conditions with and without an electric field, and humid conditions without the electric field, the catalyst presented the best performance only when the electric field was applied under humid conditions. These results suggest that the synergetic effect between 1 wt% Pd/Ce<sub>0.25</sub>Zr<sub>0.75</sub>O<sub>2</sub> and the electric field can occur at low temperatures and that it can promote the dissociation of C–H bonds of methane, even in a humid atmosphere.

### Effects of reactant gas partial pressure on methane combustion activities

To elucidate the effects of water over 1 wt% Pd/Ce<sub>0.25</sub>Zr<sub>0.75</sub>O<sub>2</sub> with the electric field, tests changing the water partial pressures were conducted. Fig. 3 presents the methane combustion activity when the water concentration was varied from 0% to 10%. Without the electric field, increasing the water concentration decreased the methane combustion activity. This result is consistent with earlier research, suggesting that the water adsorbs onto the palladium surface and forms sites such as Pd(OH)<sub>2</sub>, which are inactive for methane combustion.<sup>11,15</sup> However, the different behavior was observed when the electric field was applied. Particularly at 473–523 K, the methane conversion improved upon the addition of water. As shown in Fig. S8 (ESI†), on 1 wt% Pd/Ce<sub>0.75</sub>Zr<sub>0.25</sub>O<sub>2</sub> (not Ce<sub>0.25</sub>Zr<sub>0.75</sub>, but Ce<sub>0.75</sub>Zr<sub>0.25</sub>) catalyst, the introduction of water did not lead to improvement in methane combustion activity, irrespective of the presence or absence of the electric field, showing similar trends to earlier work. Only the 1 wt% Pd/Ce<sub>0.25</sub>Zr<sub>0.75</sub>O<sub>2</sub> catalyst demonstrates high resistance to steam, suggesting that water is involved in the methane combustion reaction process.

To confirm the characteristics of 1 wt% Pd/Ce<sub>0.25</sub>Zr<sub>0.75</sub>O<sub>2</sub> in the presence of water, the pressure dependence of each

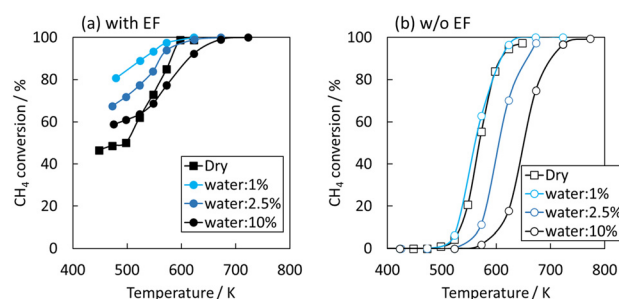


**Fig. 3** Methane conversion over 1 wt% Pd/Ce<sub>0.25</sub>Zr<sub>0.75</sub>O<sub>2</sub> with various water vapour pressures (0, 1, 2.5, 10%), (a) with the EF and (b) without the EF.



gas was examined. The reaction rate equation was estimated as shown below.

$$r = kP_{\text{CH}_4}^\alpha P_{\text{O}_2}^\beta P_{\text{H}_2\text{O}}^\gamma \quad (3)$$

Fig. S9 in ESI† depicts the reaction order of the respective gases with and without the electric field. The data are summarised in Table S3.† In the case of thermal reaction at 673 K, the reaction order of methane, oxygen, and water was 1.19,  $-0.04$ , and  $-0.70$ , which is consistent with findings from earlier studies.<sup>25–27</sup> In the electric field reaction at 473 K with 1 mA current, the reaction order of methane, oxygen, and water was 0.62,  $-0.01$ , and  $-0.16$ , representing a marked change in the water order and exhibiting improved water resistance. Based on the  $\text{H}_2\text{O}$ -TPD results presented in Table 1, most of the water was desorbed in the thermal reaction at 673 K, whereas a considerable amount of adsorbed water remained in the reaction with the electric field at 473 K. Despite this adsorption condition, the reaction order of water improved by application of the electric field from  $-0.70$  to  $-0.16$ . This result suggests activation of water by the electric field. For catalytic steam reforming of methane with the electric field, it has been confirmed that water in the system promotes proton conduction on the catalyst surface and activates methane.<sup>20,28</sup> Presumably, a similar mechanism of methane activation by water occurs in this system.

### Influence of water on methane activation

To elucidate methane activation originating from proton conduction experimentally, methane activation with steam was investigated in the electric field. Fig. S10 in ESI† presents the relation between water adsorption amount and methane activation activity with steam (473 K) given the same input power (1 W). These findings confirmed that methane activation by steam was observed even at low temperatures for all catalysts, including 1 wt% Pd/Ce<sub>0.25</sub>Zr<sub>0.75</sub>O<sub>2</sub>, indicating that the methane activation at palladium and support interface was promoted by proton conduction on the catalyst surfaces.<sup>20</sup> Additionally, these results suggest that methane activation with steam in the electric field was promoted with increased water adsorption on the catalyst, which is consistent with reported results from earlier studies.<sup>29,30</sup>

From the results obtained from partial pressure dependence and methane activation tests conducted in the electric field with steam, it was inferred that proton conduction occurs during methane combustion reactions under humid conditions, leading to an activation effect on methane. However, earlier studies of heated catalysis demonstrated that Pd tends to form Pd(OH)<sub>2</sub> in the presence of steam, leading to deactivation.<sup>11,15</sup> Therefore, these two effects might influence methane combustion activity under humid conditions in an electric field. Fig. 4 shows the ratio of methane consumption rates ( $r_{\text{CH}_4,\text{humid}}/r_{\text{CH}_4,\text{dry}}$ ) against water adsorption amount. As depicted in this figure, a decrease in water adsorption amount engenders improvement in the ratio of methane consumption rates. This reduction in water adsorption

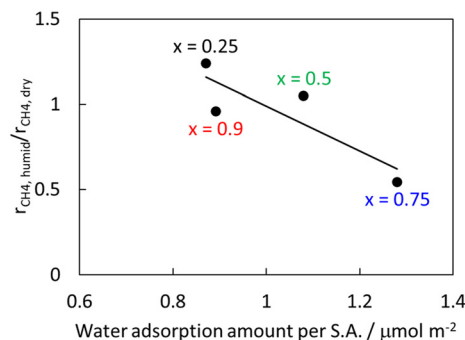
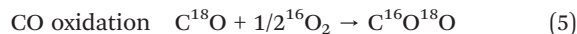


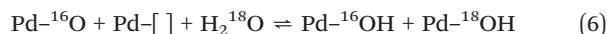
Fig. 4 Relation between water adsorption amount per surface area and the methane consumption ratio ( $r_{\text{CH}_4,\text{humid}}/r_{\text{CH}_4,\text{dry}}$ ) over 1 wt% Pd/Ce<sub>x</sub>Zr<sub>1-x</sub>O<sub>2</sub> in the EF, 473 K, 1 mA.

is assumed to inhibit Pd(OH)<sub>2</sub> formation on the catalyst surface, thereby enhancing the methane activation attributable to the electric field effects. The findings suggest that 1 wt% Pd/Ce<sub>0.25</sub>Zr<sub>0.75</sub>O<sub>2</sub> demonstrated better methane combustion activity under humid conditions than under dry conditions because its lower water adsorption amount compared to other supports reduced the formation of inactive species, consequently allowing for a greater contribution of the electric field to methane activation.

Fig. 5 exhibits test results of methane combustion activity over 1 wt% Pd/Ce<sub>0.25</sub>Zr<sub>0.75</sub>O<sub>2</sub> with the introduction of  $\text{H}_2^{18}\text{O}$ . In the reactions with the electric field (1 mA), the production of  $\text{C}^{16}\text{O}_2$  ( $m/z = 44$ ),  $\text{C}^{16}\text{O}^{18}\text{O}$  ( $m/z = 46$ ), and  $\text{C}^{18}\text{O}_2$  ( $m/z = 48$ ) was observed starting from 473 K, whereas in the thermal reactions, it was observed from 573 K. If methane activation by steam is promoted selectively in the electric field, then can be estimated that  $\text{C}^{16}\text{O}^{18}\text{O}$  is produced more abundantly than by the thermal reactions, according to the following reaction equations. However, the findings confirmed the similarity of the production ratios of  $m/z = 44$ , 46, and 48 in the thermal reactions and the reactions with the electric field.



These results suggest that methane activation was enhanced at the interface between palladium and the support with the electric field, whereas methane combustion proceeded *via* oxygen present on palladium. The presence of  $m/z = 46$  and 48 in both reaction systems likely arises from water adsorption on the Pd surface and from its equilibrium reactions.<sup>31–33</sup>



## Conclusions

This study investigated the effects of steam on complete methane combustion in an electric field. In Pd/CZO catalyst



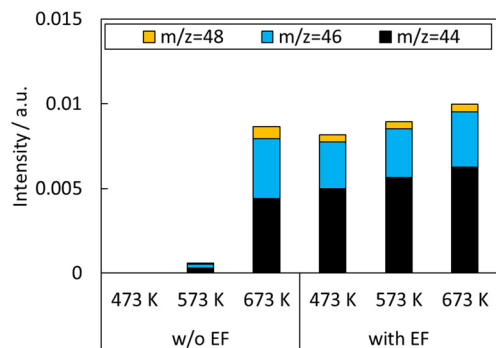


Fig. 5 Signal intensities of  $m/z = 44$  ( $C^{16}O_2$ ),  $46$  ( $C^{16}O^{18}O$ ), and  $48$  ( $C^{18}O_2$ ) over 1 wt% Pd/Ce<sub>0.25</sub>Zr<sub>0.75</sub>O<sub>2</sub> in H<sub>2</sub><sup>18</sup>O isotopic exchange tests with and w/o the EF.

systems with the electric field, 1 wt% Pd/Ce<sub>0.25</sub>Zr<sub>0.75</sub>O<sub>2</sub> exhibited the highest methane combustion activity in a humid atmosphere. Furthermore, this catalyst showed higher methane combustion activity under humid conditions than under dry conditions. H<sub>2</sub>O-TPD revealed that 1 wt% Pd/Ce<sub>0.25</sub>Zr<sub>0.75</sub>O<sub>2</sub> showed the lowest water adsorption amount, suggesting suppression of the formation of Pd(OH)<sub>2</sub>, which is inactive for methane combustion. Additionally, from results of partial pressure dependency tests and observations of activities of methane with steam in the electric field, it can be inferred that proton conduction occurs with the electric field in a humid atmosphere, consequently enhancing methane activation. Therefore, 1 wt% Pd/Ce<sub>0.25</sub>Zr<sub>0.75</sub>O<sub>2</sub> catalyst demonstrated better methane combustion activity under humid conditions than under dry conditions because its lower water adsorption amount reduced the formation of inactive species, thereby facilitating greater contributions to methane activation with the electric field.

## Data availability

The data supporting this article have been included as part of the ESI.†

## Author contributions

Conceptualisation: KS and YS, funding acquisition: YS, investigation: KS, TH, NM, project administration: YS, supervision: YS, validation: KS, TH, NM, HT, YS, visualization: KS and YS, writing – original draft: KS, writing – review & editing: YS.

## Conflicts of interest

The authors have no conflict to declare.

## Acknowledgements

STEM (JEM-ARM200F) measurements, XPS (Quantera SXM) measurements and H<sub>2</sub>O-TPD were kindly provided by N.E.

CHEMCAT Corp. A part of this work was supported by JSPS KAKENHI (grant no. 23H05404 and 23 K20034) from the Japan Society for the Promotion of Science.

## References

- P. Lott, M. Casapu, J.-D. Grunwaldt and O. Deutschmann, *Appl. Catal., B*, 2024, **340**, 123241.
- L. He, Y. Fan, J. Bellettre, J. Yue and L. Luo, *Renewable Sustainable Energy Rev.*, 2020, **119**, 109589.
- M. I. Khan, T. Yasmin and A. Shakoor, *Renewable Sustainable Energy Rev.*, 2015, **51**, 785–797.
- Z. Li and G. B. Hoflund, *J. Nat. Gas Chem.*, 2003, **12**, 153–160.
- Z. Tang, T. Zhang, D. Luo, Y. Wang, Z. Hu and R. T. Yang, *ACS Catal.*, 2022, **12**, 13457–13474.
- K. Tanaka, O. Cavalett, W. J. Collins and F. Cherubini, *Nat. Clim. Change*, 2019, **9**, 389–396.
- D. Jiang, K. Khivantsev and Y. Wang, *ACS Catal.*, 2020, **10**, 14304–14314.
- T. V. Choudhary, S. Banerjee and V. R. Choudhary, *Appl. Catal., A*, 2002, **234**, 1–23.
- J. Chen, H. Arandiyani, X. Gao and J. Li, *Catal. Surv. Asia*, 2015, **19**, 140–171.
- X. Jiang, D. Mira and D. L. Cluff, *Prog. Energy Combust. Sci.*, 2018, **66**, 176–199.
- X. Zhao, T. Chen, Y. Wang, K. Li, R. Zhan and H. Lin, *Chem. Eng. J.*, 2023, **457**, 141126.
- Z. Zhang, J. Li, T. Yi, L. Sun, Y. Zhang, X. Hu, W. Cui and X. Yang, *Chin. J. Catal.*, 2018, **38**, 1228–1239.
- P. Gélin and M. Primet, *Appl. Catal., B*, 2002, **39**, 1–37.
- X. Feng, L. Jiang, D. Li, S. Tian, X. Zhu, H. Wang, C. He and K. Li, *J. Energy Chem.*, 2022, **75**, 173–215.
- R. S. Kumar, R. E. Hayes and N. Semagina, *Catal. Today*, 2021, **382**, 82–95.
- M. Heintze and B. Pietruszka, *Catal. Today*, 2004, **89**, 21–25.
- C. G. Vayenas and C. G. Koutsodontis, *J. Chem. Phys.*, 2008, **128**, 182506.
- Y. Sekine, M. Tomioka, M. Matsukata and E. Kikuchi, *Catal. Today*, 2009, **146**, 183–187.
- Y. Sekine, M. Haraguchi, M. Tomioka, M. Matsukata and E. Kikuchi, *J. Phys. Chem. A*, 2010, **114**, 3824–3833.
- R. Manabe, S. Okada, R. Inagaki, K. Oshima, S. Ogo and Y. Sekine, *Sci. Rep.*, 2016, **6**, 38007.
- K. Sugiura, S. Ogo, K. Iwasaki, T. Yabe and Y. Sekine, *Sci. Rep.*, 2016, **6**, 25154.
- A. Shigemoto, Y. Inoda, C. Ukai, T. Higo, K. Oka and Y. Sekine, *Chem. Commun.*, 2024, **60**, 1563–1566.
- A. Shigemoto, T. Higo, Y. Narita, S. Yamazoe, T. Uenishi and Y. Sekine, *Catal. Sci. Technol.*, 2022, **12**, 4450–4455.
- K. Li, K. Liu, H. Ni, B. Guan, R. Zhan, Z. Huang and H. Lin, *Mol. Catal.*, 2018, **459**, 78–88.
- F. H. Ribeiro, M. Chow and R. A. Della-Betta, *J. Catal.*, 1994, **146**, 537–544.



- 26 J. C. van Giezen, F. R. van den Berg, J. L. Kleinen, A. J. van Dillen and J. W. Geus, *Catal. Today*, 1999, **47**, 287–293.
- 27 K. Murata, J. Ohyama, Y. Yamamoto, S. Arai and A. Satsuma, *ACS Catal.*, 2020, **10**, 8149–8156.
- 28 S. Okada, R. Manabe, R. Inagaki, S. Ogo and Y. Sekine, *Catal. Today*, 2018, **307**, 272–276.
- 29 A. Takahashi, R. Inagaki, M. Torimoto, Y. Hisai, T. Matsuda, Q. Ma, J. G. Seo, T. Higo, H. Tsuneki, S. Ogo, T. Norby and Y. Sekine, *RSC Adv.*, 2020, **10**, 14487.
- 30 M. Torimoto, S. Ogo, Y. Hisai, N. Nakano, A. Takahashi, Q. Ma, J. G. Seo, H. Tsuneki, T. Norby and Y. Sekine, *RSC Adv.*, 2020, **10**, 26418.
- 31 K. Fujimoto, F. H. Ribeiro, M. Avalos-Borja and E. Iglesia, *J. Catal.*, 1998, **179**, 431–442.
- 32 X. Li, X. Wang, K. Roy, J. A. van Bokhoven and L. Artiglia, *ACS Catal.*, 2020, **10**, 5783–5792.
- 33 K. Nagakawa, H. Sampei, A. Takahashi, J. Sasaki, T. Higo, N. Mori, H. Sato and Y. Sekine, *RSC Adv.*, 2022, **12**, 25565–25569.

